Aerobic Titania Photocatalysis: Selective Oxidative Dehydrogenation of Tetrahydroisoquinoline and Related Amines

Paula Romero-Navarro, Iris Martín-García, Anabel Lanterna,
Juan C. Scaiano and Francisco Alonso*

Supplementary Information

1. General

Anhydrous copper(II) chloride (97%, Aldrich), lithium powder (MEDALCHEMY S. L.), DTBB (4,4'-di-*tert*-butylbiphenyl, Aldrich), TiO_2 (P25 Degussa Evonik; Merck), and all other reagents (Merck, Acros, Alfa Aesar, Fluorochem) were commercially available of the best grade and were used without further purification. THF was dried in a Sharlab PS-400-3MD solvent purification system using an alumina column. MQuant Peroxide Test Method: colourimetric with test strips 1-3-10-30-100 mg/L H_2O_2 (Merck).

The TEM images were recorded with a JEOL JEMM2010 microscope, equipped with a lanthanum hexaboride filament operated at an acceleration voltage of 200 kV. For their observations, the as-prepared samples were mounted on holey-carbon coated gold grids. The size distribution of the CuNPs was determined by TEM. EDX analyses were carried out with an Oxford Inca Energy TEM100 attachment. The XPS spectra were measured with a VG-Microtech Multilab 3000 electron spectrometer using a non-monochromatised Al-Kα (1486.6 eV) radiation source of 300 W and a hemispheric electron analyser equipped with 9 channeltron electron multipliers. The pressure inside the analysis chamber during the scans was about $5 \cdot 10^{-7}$ N/m^2. Higher resolution survey scans were performed at a pass energy of 50 eV. The intensities of the different contributions were obtained by means of the calculation of the integral of each peak, after having eliminated the baseline with S form and adjusting the experimental curves to a combination of Lorentz (30%) and Gaussian (70%) lines. All the binding energies were referred to the line of the C 1s to 284.4 eV, obtaining values with a precision of ± 0.2 eV. Diffuse Reflectance (DR) measurements were performed with an Agilent Cary 7000 UV-Vis-NIR Universal Measurement Spectrophotometer coupled with an Agilent Praying Mantis accessory (Scaiano's laboratory). ICP-OES analyses were performed with a Perkin Elmer Optima 4300 DV (dual vision) apparatus and ICP-MS analyses were carried out with Thermo Elemental VG PQ-ExCell instrument, using in both cases the Cetac model U5000AT+ as an ultrasonic nebulizer. Infrared analysis was performed with a Jasco 4100LE (Pike MIRacle ATR) spectrophotometer; wavenumbers (ṽ) are given in cm^{-1}. NMR spectra were recorded on a Bruker Avance 400 spectrometer (400 MHz for ^{1}H NMR; 101 MHz for ^{13}C NMR); chemical shifts are given in (δ) parts per million (ppm) and coupling constants (J) in Hertz. Mass spectra (EI) were obtained at 70 eV on Agilent 5763 (GC) spectrometer; fragment ions in *m/z* with relative intensities (%) in parentheses. HRMS analyses (EI) were also carried out at 70 eV on an Agilent 7200 (Q-TOF) spectrometer. The purity of volatile compounds and the chromatographic analyses (GLC) were determined with a Youling 6100 instrument equipped with a flame ionisation detector and a HP-5MS 30 m capillary column (0.25 mm diameter, 0.25 μm film thickness), using nitrogen (1 mL/min) as carrier gas, $T_{injector}$ = 270 ºC, T_{column} = 60 ºC (3 min) and 60–270 ºC (15 ºC/min); retention times (t_R) are given in min. Analytical thin-layer chromatography (TLC) was carried out on TLC plastic sheets

with silica gel 60 F254 (Merck). Column chromatography was performed using silica gel 60 of 40–60 microns (hexane-EtOAc as eluent).

All reactions were carried out on a multireactor apparatus using the corresponding reactor tubes equipped with LZ4-04UV00 UV LEDs (365 nm, 3.30 W at 700 mA). The light power was measured using the StellarNet BLUE-wave UV-Vis spectrometer (300-1100 nm wavelength range) equipped with a USB-2 interface with a snapshot memory to provide instantaneous spectral images from a highly sensitive CCD detector with 2048 elements. A single strand fibre optic cable (diameter = 600 µm, length = 2.00 m) delivers input via a standard SMA 905 fibre optic connector. The information was analysed employing the Spectrawiz software included in the USB 2.0.

2. Typical procedure for the preparation of the TiO_2-supported photocatalysts

Anhydrous copper(II) chloride (134 mg, 1.0 mmol) was added to a deep green suspension of lithium powder (14 mg, 2.0 mmol) and 4,4'-di-*tert*-butylbiphenyl (DTBB, 27 mg, 0.1 mmol) in dry THF (2 mL), at room temperature under an argon atmosphere. The reaction mixture suddenly changed to black indicating that the CuNPs suspension was formed. This mixture was diluted with additional dry THF (18 mL) followed by the addition of TiO_2 (1.28 g). The resulting mixture was stirred for 1 h at room temperature, filtered, and the grey solid was successively washed with MeOH (5 mL) and THF (20 mL), and dried in air for 24 h. The preparation of the bimetallic catalysts supported on TiO_2 followed the same strategy as above, but starting from an equimolecular mixture of the metal salts.

3. Bandgap energy measurements

The bandgap energy (E_g) of the different catalysts was determined *via* Diffuse Reflectance Spectroscopy (DRS) with a suitable UV-Vis spectrophotometer and ignoring specular reflection. First, the absorption coefficient F(R) (proportional to the extinction coefficient) was calculated according to the Kubelka-Munk equation,[1] where R is the reflectance of the sample; then, F(R) *versus* wavelength was plotted for all catalysts (Figure S1).

$$F(R) = \frac{(1-R)^2}{2R}$$

The E_g of the semiconductor particles can be obtained by plotting the modified Kubelka-Munk function $[F(R)\ h\nu]^{1/n}$ as a function of the energy in eV, according to the equation below, when extrapolating the slope to zero: A is the absorption constant and n is ½ or 2 for direct and indirect allowed transitions, respectively. Nonetheless, the $h\nu$ factor in $[F(R)\ h\nu]^{1/n}$ has been omitted sometimes because of its minor contribution to the final E_g value.[2]

$$[F(R)\ h\nu]^{1/n} = A(h\nu - E_g)$$

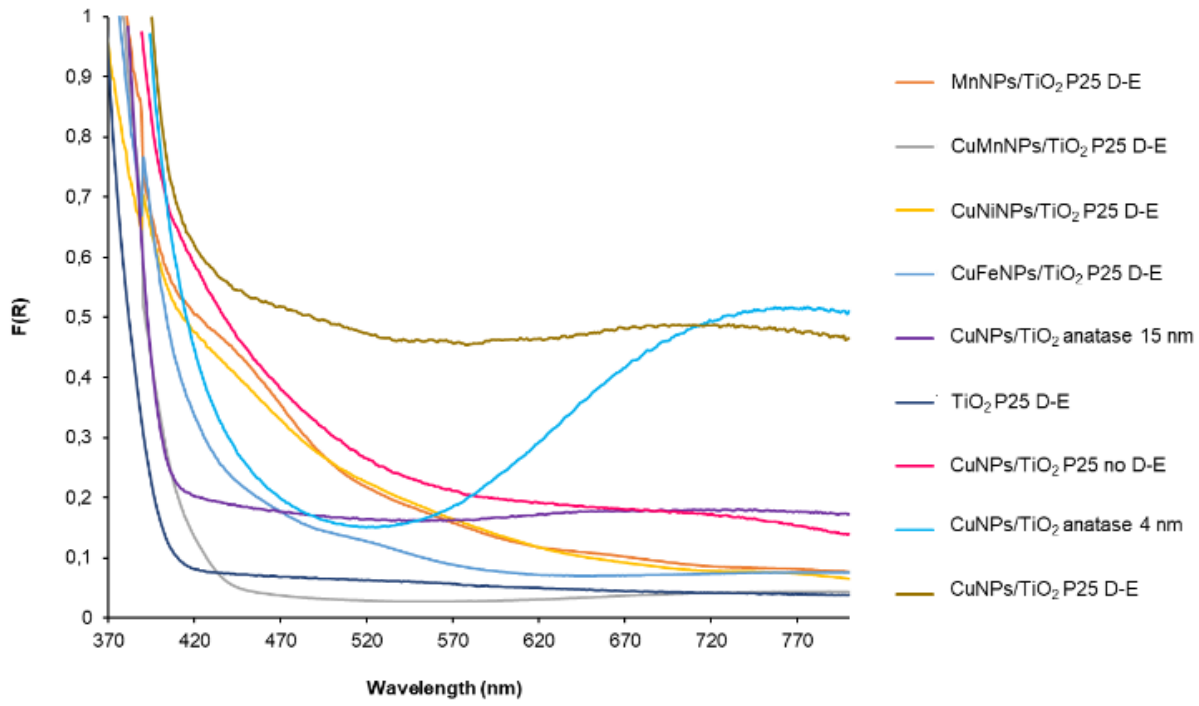

Figure S1. UV-Vis diffuse reflectance spectra [Kubelka–Munk function, F(R)] of TiO_2 and MNPs/TiO_2; D-E = Degussa-Evonik.

In order to determine the most suitable representation for our photocatalytic systems, we carried out the DR experiment with TiO_2 (P25 D-E) and plotted F(R) *vs* E_g, $[F(R)\ h\nu]^2$ *vs* E_g and $[F(R)\ h\nu]^{1/2}$ *vs* E_g, obtaining bandgap energies of 3.20, 3.55 and 3.01 eV, respectively. Given that the closest to the reported E_g value of TiO_2 (P25 D-E) was obtained with the F(R) *vs* E_g plot, the latter representation was used as a good approximation for the measurement of the rest of the bandgap energies.

4. General procedures

4.1. General procedure for the photocatalysed oxidative dehydrogenation of THIQ (1)

1,2,3,4-Tetrahydroisoquinoline (**1**) was added to a reactor tube containing the photocatalyst in a solvent under the specified atmosphere. The reaction mixture was irradiated with LEDs of 369 nm or 450–455 nm (at a given power density) during the specified time at room temperature. The resulting mixture was diluted with EtOAc, filtered through Celite/$MgSO_4$, and the reaction crude was subjected to GLC analysis.

4.2. Typical procedure for the photocatalysed oxidative dehydrogenation of THIQ (1) with CuNPs/TiO_2-P25

1,2,3,4-Tetrahydroisoquinoline (**1**, 0.5 mmol) was added to a reactor tube containing CuNPs/TiO_2-P25 (10 mg) in MeCN (2 mL) under an oxygen atmosphere (balloon). The reaction mixture was irradiated with a LED of 369 nm (0.14 W/cm^2) for 3 or 23 h at room temperature. The resulting mixture was diluted with EtOAc (2 mL), filtered through Celite/$MgSO_4$, and the reaction crude was subjected to GLC analysis. For reuse purposes, 20 mg of CuNPs/TiO_2-P25 were used in the experiments, irradiating the reaction mixture for 16 h; the photocatalyst was recovered after centrifugation and drying in air. The same reutilisation protocol was applied to TiO_2-P25 and TiO_2-P25–Cs_2CO_3.

4.3. General procedure for the photocatalysed synthesis of compounds 2–10 with TiO_2-P25 and CuNPs/TiO_2-P25

The corresponding amine (0.5 mmol) was added to a reactor tube containing TiO_2-P25 (10 mg) or CuNPs/TiO_2-P25 (10 mg) in MeCN (2 mL) under an oxygen atmosphere (balloon). The reaction mixture was irradiated with a LED of 369 nm (0.14 W/cm^2) for 24 h at room temperature. The resulting mixture was diluted with EtOAc (2 mL), filtered through Celite/$MgSO_4$, and the reaction crude was subjected to column chromatography (silica gel, hexane-EtOAc) to give the purified products **2**–**10**.

4.4. H_2O_2 detection test. Procedure A. 1,2,3,4-Tetrahydroisoquinoline (**1**, 0.5 mmol) and KI (0.5 mmol) were added to a reactor tube containing TiO_2-P25 or CuNPs/TiO_2-P25 (10 mg) in MeCN (2 mL) under oxygen. The reaction mixture was irradiated with a LED of 369 nm (0.14 W/cm^2) for 20 h at room temperature. The resulting mixture was diluted with EtOAc (2 mL), filtered through Celite/$MgSO_4$, and the reaction crude was subjected to GLC analysis.

4.5. H_2O_2 detection test. Procedure B. H_2O_2 detection was analysed by MQuant Peroxide Test Method (strips). After the typical procedure for the oxidation of 1,2,3,4-tetrahydroisoquinoline (**1**) with TiO_2-P25 or CuNPs/TiO_2-P25, an aliquot of the reaction crude was taken and dropped over the corresponding strips, followed by observation of a colour change.

5. Characterisation of compounds 2–10

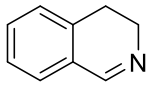

3,4-Dihydroisoquinoline (2)

Yellow oil (53.7 mg, 0.41 mmol, 82%); $\mathbf{R_f}$ 0.40 (hexane-EtOAc, 8:2); $\mathbf{t_R}$ 8.71; **IR (neat)** $\tilde{\nu}$ 3012, 1612, 1581, 1525, 1398, 1310, 1265, 1233, 1101, 1105, 822, 804, 743, 702; **^{1}H NMR** (400 MHz, $CDCl_3$) δ 8.26 (br t, J = 2.0; 1H), 7.28 (td, J = 7.2, 2.0; 1H), 7.25–7.17 (m, 2H), 7.10–7.06 (dt, J = 7.2, 0.6; 1H), 3.70 (td, J = 8.3, 2.0 Hz; 2H), 2.67 (t, J = 8.3; 2H); **^{13}C NMR (101 MHz, $CDCl_3$)** δ 160.8, 136.8, 131.5, 128.9, 127.8, 127.6, 127.5, 47.8, 25.4; **GC–MS (EI)** *m/z* 132 (M^++1, 10), 131 (M^+, 100); **HRMS (EI)** *m/z* calcd. for C_9H_9N 131.0745, found 131.0748.

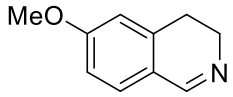

6-Methoxy-3,4-dihydroisoquinoline (4)

Yellow oil (57.8 mg, 0.36 mmol, 72%); $\mathbf{R_f}$ 0.80 (hexane-EtOAc, 8:2); $\mathbf{t_R}$ 8.93; **IR (neat)** $\tilde{\nu}$ 3005, 1606, 1571, 1500, 1462, 1433, 1308, 1275, 1252, 1155, 1124, 1032, 852, 810, 723, 669; **^{1}H NMR (400 MHz, $CDCl_3$)** δ 7.21 (d, J = 8.3 Hz; 1H), 6.70–6.65 (m, 2H), 6.62 (s, 1H), 3.76 (s, 3H), 3.11 (br s, 2H), 2.77–2.70 (m, 2H); **^{13}C NMR (101 MHz, $CDCl_3$)** δ 161.8, 158.0, 135.9, 129.1, 127.3, 113.2, 112.3, 55.3, 47.7, 29.5; **GC–MS (EI)** *m/z* 162 (M^++1, 33), 161 (M^+, 100), 160 (70), 146 (56), 134 (13), 117 (17), 91 (14); **HRMS (EI)** *m/z* calcd. for $C_{10}H_{11}NO$ 161.0841, found 161.0839.

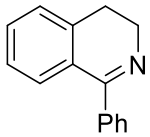

1-Phenyl-3,4-dihydroisoquinoline (5)

Yellow oil (57.0 mg, 0.275 mmol, 55%); $\mathbf{R_f}$ 0.75 (hexane-EtOAc, 8:2); $\mathbf{t_R}$ 11.05; **IR (neat)** $\tilde{\nu}$ 3112, 1672, 1604, 1495, 1456, 1311, 1120, 955, 889, 738; **^{1}H NMR (400 MHz, $CDCl_3$)** δ 7.28–7.15 (m, 9H), 3.77 (t, J = 7.3 Hz; 2H), 2.77–2.70 (m, 2H); **^{13}C NMR (101 MHz, $CDCl_3$)** δ 167.3, 135.3, 130.7, 129.3, 129.0, 128.8, 128.1, 127.9, 127.4, 126.5, 126.3, 47.6, 26.3; **GC–MS (EI)** *m/z* 207 (M^+, 95), 206 (100), 179 (35), 178 (55), 128 (10), 102 (18), 77 (10); **HRMS (EI)** *m/z* calcd. for $C_{15}H_{13}N$ 207.1048, found 207.1035.

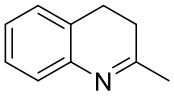

2-Methyl-3,4-dihydroquinoline (6)

The isolation of pure compound **6** was problematic because it underwent oxidation to the corresponding quinoline during chromatographic purification. $\mathbf{R_f}$ 0.75 (hexane-EtOAc, 8:2); $\mathbf{t_R}$ 8.90; **GC–MS (EI)** *m/z* 146 (M^++1, 30), 145 (M^+, 100), 131 (30); **HRMS (EI)** *m/z* calcd. for $C_{10}H_{11}N$ 145.0891, found 145.0893.

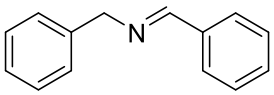

(*E*)-*N*-Benzyl-1-phenylmethanimine (7)

Brown oil (58.5 mg, 0.30 mmol, 60%); $\mathbf{R_f}$ 0.80 (hexane-EtOAc, 8:2); $\mathbf{t_R}$ 10.13; **IR (neat)** $\tilde{\nu}$ 3012, 1672, 1654, 1502, 1411, 1295, 1041, 832, 795, 718; **^{1}H NMR (400 MHz, $CDCl_3$)** δ 8.30 (s, 1H), 7.72–7.68 (m, 2H), 7.33 (dd, *J* = 5.1, 1.8 Hz; 2H), 7.25–7.23 (m, 5H), 7.19–7.16 (m, 1H), 3.73 (s, 2H); **^{13}C NMR (101 MHz, $CDCl_3$)** δ 162.4, 140.3, 131.1, 129.0, 128.9, 128.8, 128.6, 128.4, 127.4, 65.4; **GC–MS (EI)** *m/z* 195 (M^+, 81), 194 (79), 118 (12), 117 (23), 91 (100), 89 (14); **HRMS (EI)** *m/z* calcd. for $C_{14}H_{13}N$ 195.1145, found 195.1148.

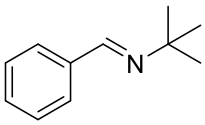

(*E*)-*N*-*tert*-Butyl-1-phenylmethanimine (8)

Yellow oil (44.3 mg, 0.275 mmol, 55%); $\mathbf{R_f}$ 0.80 (hexane-EtOAc, 8:2); $\mathbf{t_R}$ 6.42; **IR (neat)** $\tilde{\nu}$ 3102, 2967, 1641, 1452, 1362, 1227, 1205, 696; **^{1}H NMR (400 MHz, $CDCl_3$)** δ 8.20 (s, 1H), 7.69–7.64 (m, 2H), 7.26–7.18 (m, 3H), 1.11 (s, 9H); **^{13}C NMR (101 MHz, $CDCl_3$)** δ 155.2, 137.2, 128.4, 127.9, 126.8, 57.2, 29.1; **GC–MS (EI)** *m/z* 161 (M^+, 12), 147 (16), 146 (100), 106 (22), 104 (21), 57 (16); **HRMS (EI)** *m/z* calcd. for $C_{11}H_{15}N$ 161.1224, found 161.1220.

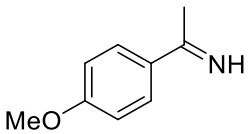

1-(4-Methoxyphenyl)ethan-1-imine (9)

Yellow oil (43.3 mg, 0.29 mmol, 58%); $\mathbf{R_f}$ 0.8 (hexane-EtOAc, 8:2); $\mathbf{t_R}$ 10.31; **IR (neat)** $\tilde{\nu}$ 2967, 1652, 1438, 1421, 1338, 1205, 711, 592; **^{1}H NMR (400 MHz, $CDCl_3$)** δ 7.77 (brs, 1H), 7.58, 6.90 (AA'XX' system, *J* = 9.1; 4H), 3.83 (s, 3H), 2.26 (s, 3H); **^{13}C NMR (101 MHz, $CDCl_3$)** δ 160.9,

156.2, 129.6, 127.8, 114.3, 55.8, 12.4; **GC–MS (EI)** *m/z* 149 (M^+, 15), 148 (23), 134 (100), 118 (52); **HRMS (EI)** *m/z* calcd. for $C_9H_{11}NO$ 149.0891, found 149.0882.

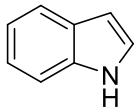

1*H*-Indole (10)

Yellow oil (35.1 mg, 0.30 mmol, 60%); $\mathbf{R_f}$ 0.60 (hexane-EtOAc, 8:2); $\mathbf{t_R}$ 7.18; **IR (neat)** $\tilde{\nu}$ 3411, 1690, 1581, 1483, 1454, 1414, 1334, 1277, 1265, 1092, 1065, 1007, 739; **^{1}H NMR (400 MHz, $CDCl_3$)** δ 7.88 (s, 1H), 7.59–7.54 (m, 1H), 7.27–7.22 (m, 1H), 7.14–7.07 (m, 1H), 7.07–7.01 (m, 2H), 6.46 (ddd, J = 3.1, 2.0, 0.9 Hz; 1H); **^{13}C NMR (101 MHz, $CDCl_3$)** δ 135.9, 128.0, 124.3, 122.1, 120.8, 119.9, 111.2, 102.7; **GC–MS (EI)** *m/z* 117 (M^+, 100), 90 (32), 89 (23), 63 (10); **HRMS (EI)** *m/z* calcd. for C_8H_7N 117.0548, found 117.0540.

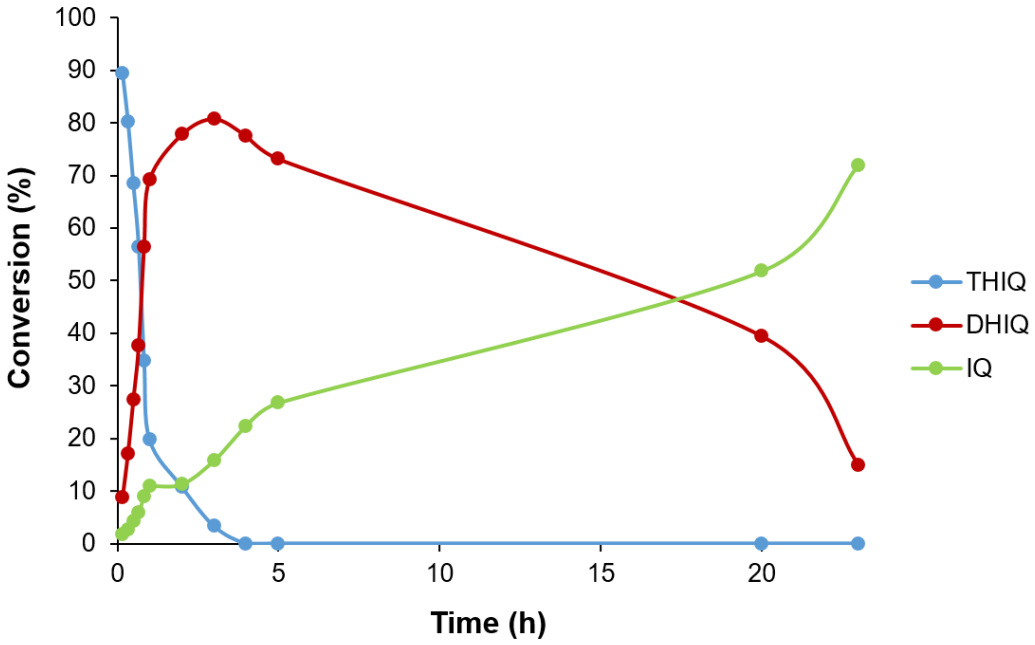

Figure S2. Reaction profile for the oxidative dehydrogenation of THIQ (**1**, 0.5 mmol) photocatalysed (369 nm LED) by TiO_2-P25 (10 mg) in MeCN (2 mL) under an O_2 atmosphere.

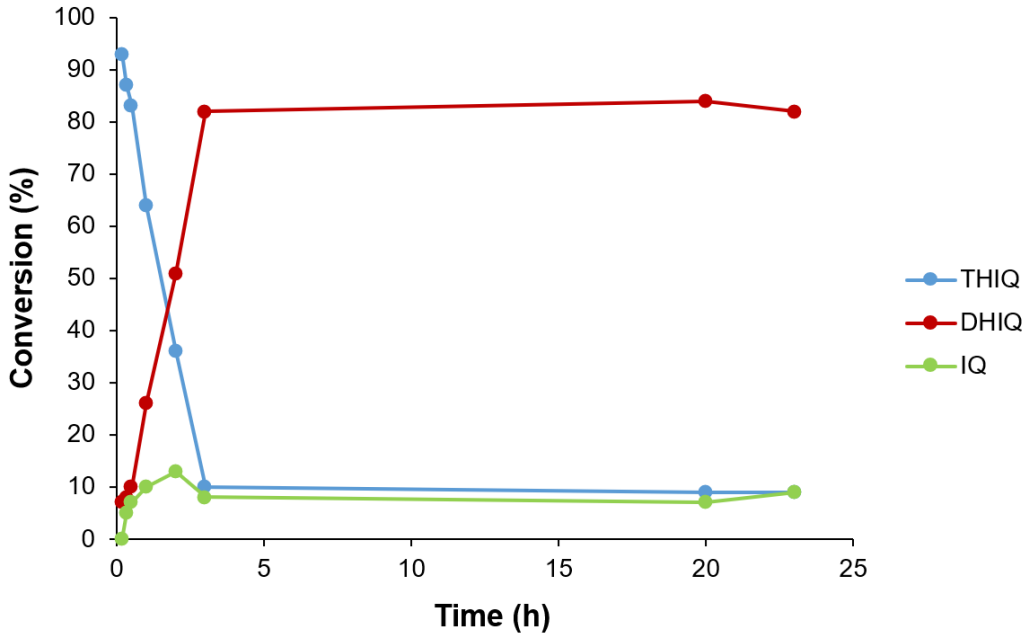

Figure S3. Reaction profile for the oxidative dehydrogenation of THIQ (**1**, 0.5 mmol) photocatalysed (369 nm LED) by CuNPs/TiO_2-P25 (10 mg) in MeCN (2 mL) under an O_2 atmosphere.

Table S1. Reuse of the three best photocatalysts in the oxidative dehydrogenation of THIQ (**1**).[a]

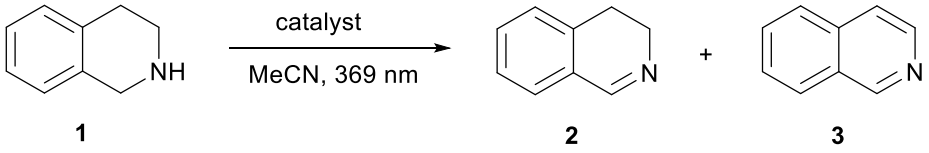

1 **2** **3**

Entry	Catalyst	Base-atmosphere	Conversion (%)[b]	Selectivity **2**/**3** (%)[b]
1	TiO_2-P25	O_2	95, 65, 50	82, 80, 82
2	TiO_2-P25	Cs_2CO_3[c]-air	92, 60, 48	91, 90, 80
3	CuNPs/TiO_2-P25	O_2	90, 90, 91	91, 91, 93
4	TiO_2-P25	O_2	>99, 95, 85	84, 79, 39
5	TiO_2-P25	Cs_2CO_3[c]-air	91, 88, 70	82, 77, 50
6	CuNPs/TiO_2-P25	O_2	97, 97, 95, 96, 75[d]	97, 97, 97, 96, 95

[a] Reaction conditions: **1** (0.5 mmol), catalyst (10 mg, entries 1–3; 20 mg, entries 4–6), MeCN (2 mL), LED 369 nm (0.14 W/cm^2). [b] Conversions of THIQ (**1**) into DHIQ (**2**) and IQ (**3**), and selectivities for 3–5 consecutive cycles were determined by GLC after 3 h (entries 1–3) or 16 h (entries 4–6). [c] 1 equiv. [d] Formation of the lactam of **1** [3,4-dihydroisoquinolin-1(2*H*)-one] was observed.

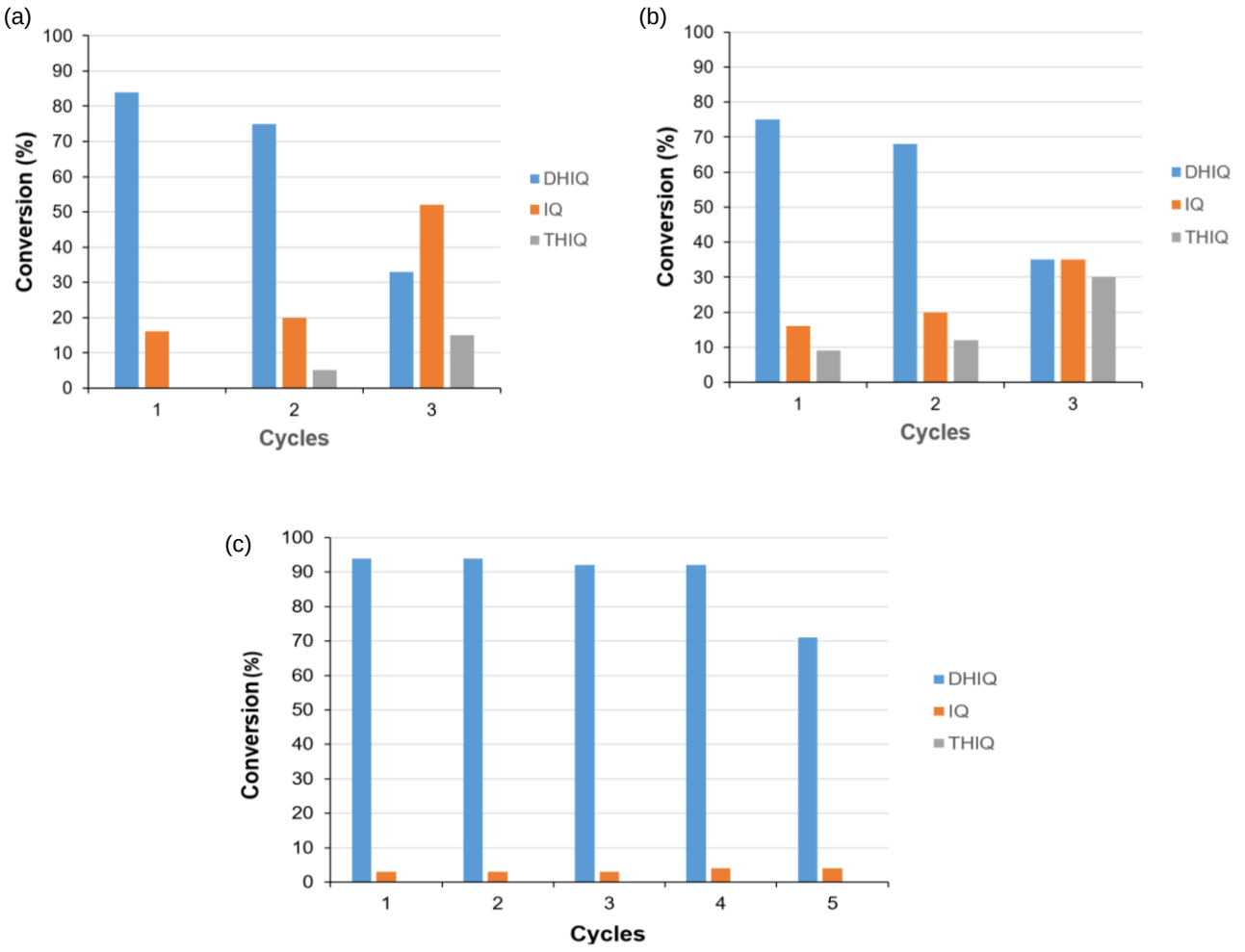

Figure S4. Reuse of (a) TiO_2-P25, (b) TiO_2-P25–Cs_2CO_3, and (c) CuNPs/TiO_2-P25 in the photocatalysed oxidative dehydrogenation of THIQ (**1**). See the conditions in Table S1.

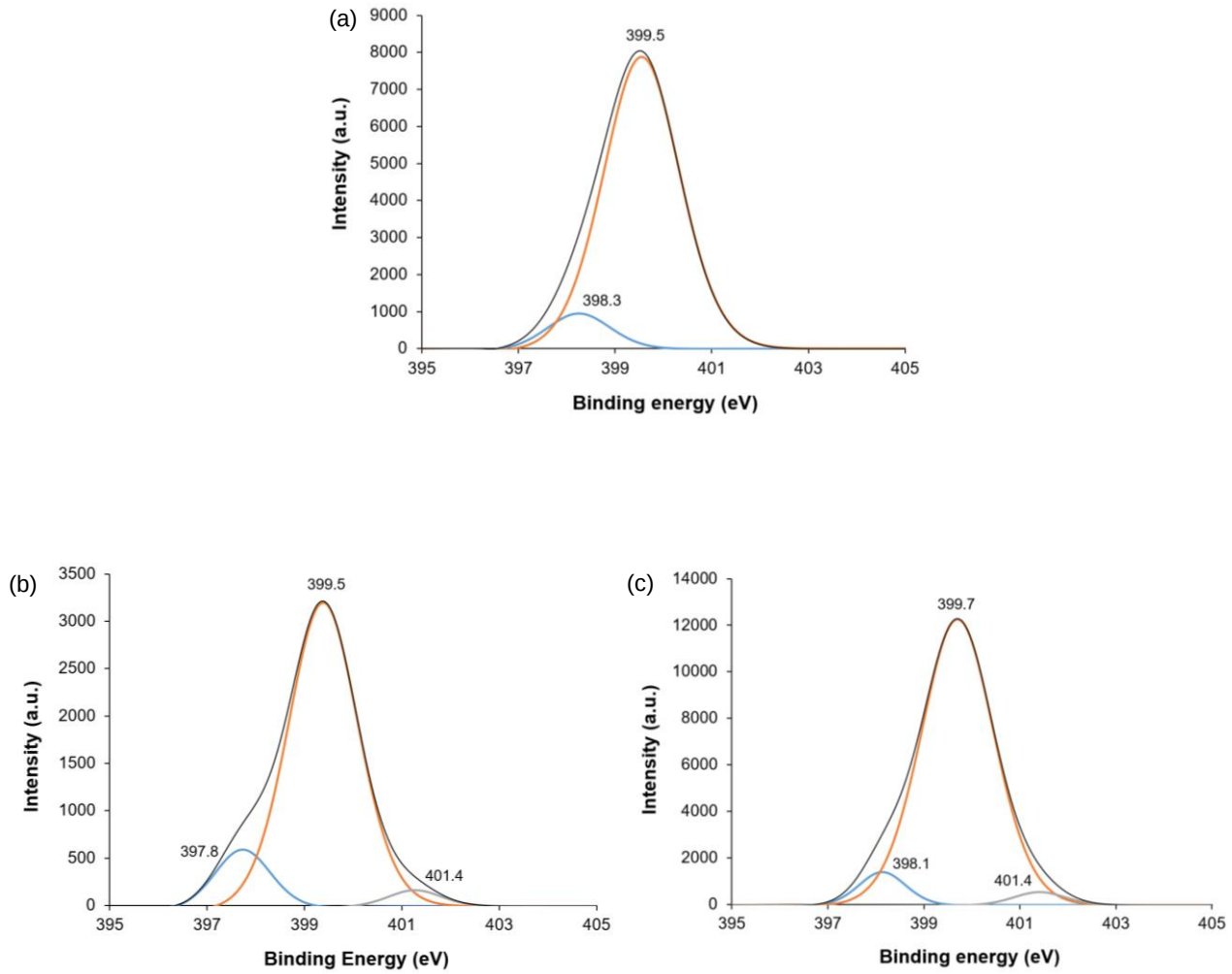

Figure S5. XPS spectra at the N 1*s* level of: (a) TiO_2-P25 (10 mg) after the third run (3 h); CuNPs/TiO_2-P25 (20 mg) after the first (b) and fifth (c) runs (20 mg, 16 h).

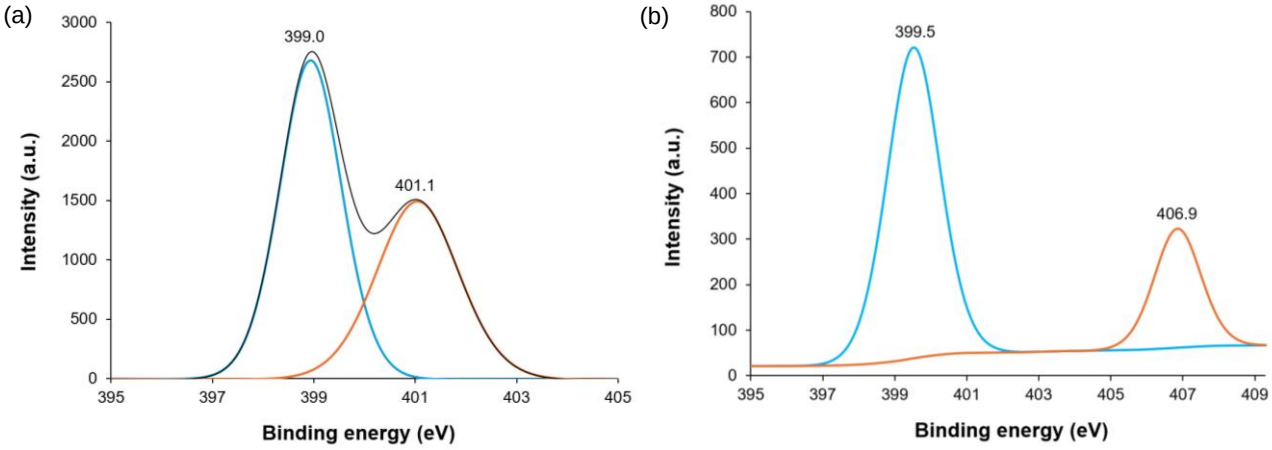

Figure S6. XPS spectra at the N 1*s* level of (a) TiO_2-P25 and (b) CuNPs/TiO_2-P25 impregnated with THIQ (**1**).

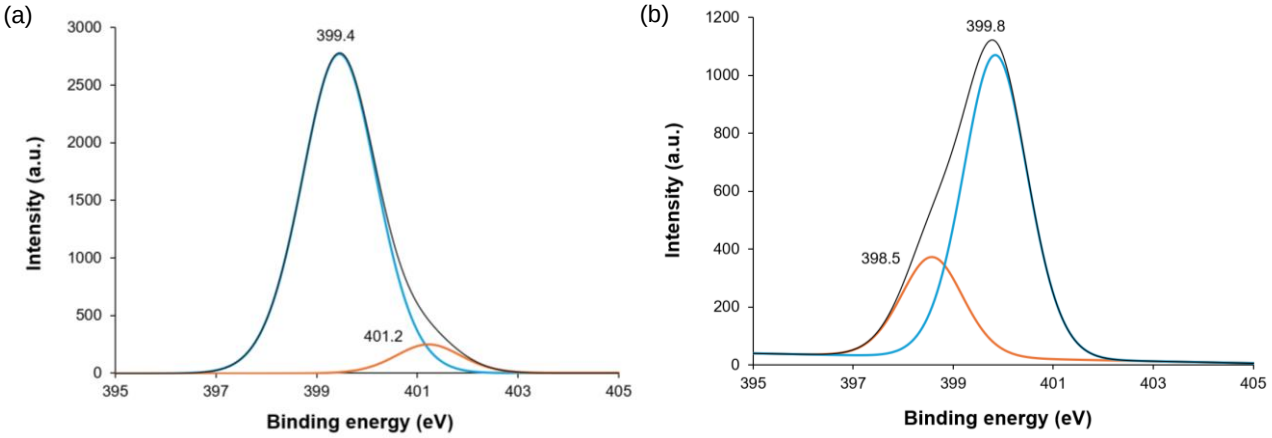

Figure S7. XPS spectra at the N 1*s* level of (a) TiO_2-P25 and (b) CuNPs/TiO_2-P25 impregnated with DHIQ (**2**).

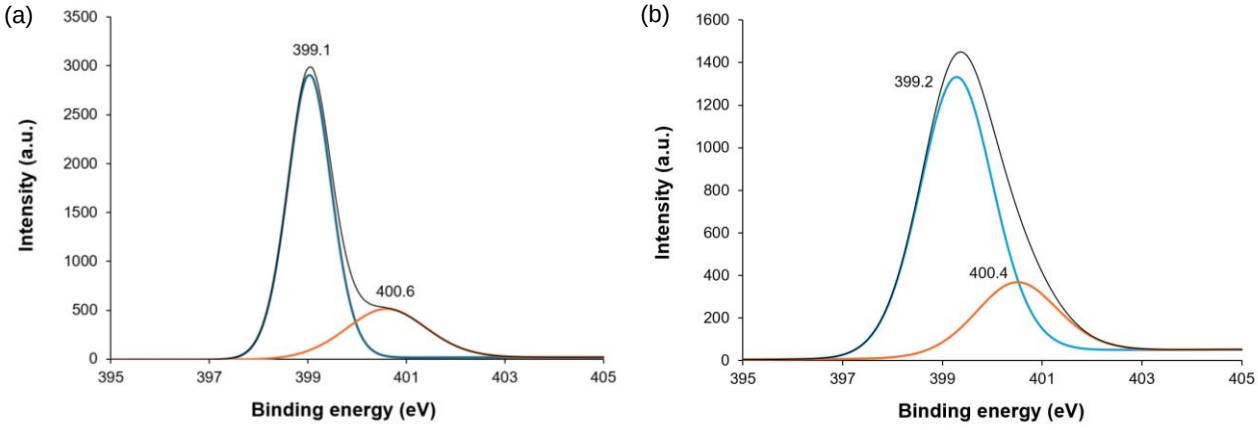

Figure S8. XPS spectra at the N 1*s* level of (a) TiO_2-P25 and (b) CuNPs/TiO_2-P25 impregnated with IQ (**3**).

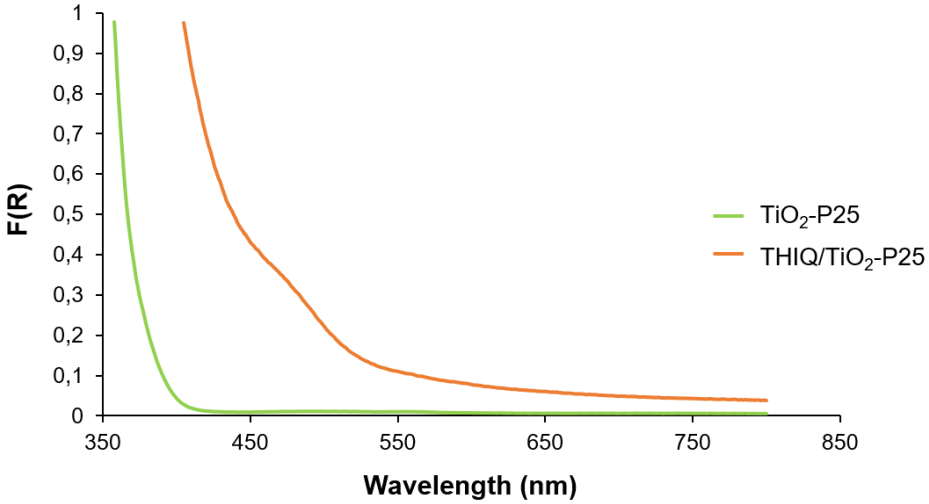

Figure S9. UV-Vis diffuse reflectance spectra [Kubelka–Munk function, F(R)] of TiO_2-P25 and TiO_2-P25 impregnated with THIQ (**1**).

Table S2. Comparison with other catalysts: conditions and performance.

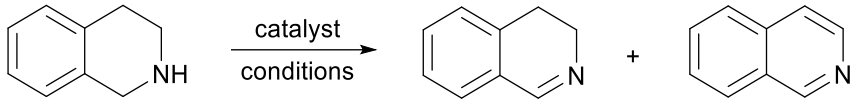

1 2 3

Entry	Catalyst	Light	Conditions	2 (%)[a]	Ref.
1	Porphyrinic Zr-MOF	300 W xenon lamp (>420 nm)	MeCN, rt, 70 min, air	100 yield	3
2	Tetraphenylporphyrin	300 W tungsten lamp	MS 4Å, EtOAc, rt, 8 h, O_2	97 yield	4
3	Co-thioporphyrazine	Xe lamp (>420 nm)	MeCN, rt, 8 h, O_2	38 conv. 72 select.	5
4	Zn(II)-chlorin complex	Xe lamp (>400 nm)	MS 4Å, BTF, rt, 0.5 h, 0.1 MPa O_2	87 yield	6
5	Chromophore-cobaloxime	3 W 16 blue LEDs (450 nm)	THF, rt, 12 h, N_2	86 yield 96 select.	7
6	Porous organic polymer[b]	30 W green LED lamp (520 nm)	MeCN, 25 ºC, 10 h, O_2	99 yield	8
7	Microporous carbazolic polymer	150 W Xe lamp	MeCN, 10 ºC, 10 h, O_2	72 yield	9
8	C_{70}	200 W tungsten lamp (white light)	MS 4Å, $CHCl_3$, 4 h, O_2	>99 yield	10
9	CO_2, eosin Y	12 W blue LED	DBN, DMSO, 48 h, 25-30 ºC	87 yield	11
10	Bodipy derivative	35 W xenon lamp (>380 nm)	MeCN, 22 ºC, 2.5 h, air	74 yield	12
11	mpg-C_3N_4	300 W Xe lamp (>420 nm)	MeCN, 80 ºC, 2 h, 0.5 MPa O_2	99 conv. 91 select.	13
12	g-C_3N_4/BiOBr	50 W LED lamp (>400 nm)	MeCN, 27-29 ºC, 2 h, O_2	76 conv. 61 yield	14
13	$Bi_2O_2CO_3$	300 W Xe lamp	MeCN, 25 ºC, 6 h, 0.3 MPa O_2	100 conv. 88 select.	15
14	Zn-MOF	LEDs (660 nm)	MeCN, 60 ºC, 24 h, 0.1 MPa O_2	18 conv.	16
15	$[Ru(bpy)_3](PF_6)_2$	11 W white LED bulb	TBHP, MeCN, 1 h, rt	80 yield	17
16	$[Ru(bpy)_3](PF_6)_2$	23 W CFL	MS 4Å, Na_3PO_4, MeCN, 35 ºC, 48 h	>99 conv. 43 yield	18
17	Nb_2O_5	500 W Hg lamp (>300 nm)	benzene, rt, 11 h, O_2	99 conv. 92 select.	19
18	$MoS_2/ZnIn_2S_4$	5 W 9 Vis LEDs	MeCN-H_2O, rt, 12 h, N_2	94 conv. 90 select.	20
19	TiO_2 anatase	300 W Xe lamp (>420 nm)	MeCN, 40 ºC, 5 h, air	100 conv. 68 select.	21
20	Pt/TiO_2	Xe lamp	MeCN, 25 ºC, 16 h, 0.3 MPa N_2	30 conv. 70 select.	22
21	$Ni(NO_3)_2/TiO_2$	blue LED (453 nm)	4-amino-TEMPO *i*-PrOH, rt, 24 h, O_2	52 yield	23
22	Rh/TiO_2	blue LED (453 nm)	*i*-PrOH, rt, 48 h, Ar	48 yield	24
23	TiO_2-P25	3 W LED (369 nm)	MeCN, rt, 16 h, O_2	>99 conv. 84 select.	this work
24	CuNPs/TiO_2-P25	3 W LED (369 nm)	MeCN, rt, 16 h, O_2	97 conv. 97 select.	this work

[a] Yield, conversion and selectivity are provided according to what is available in the references. [b] The polymer is based on 2,7-bis-(*N*-carbazolyl)-9-fluorenone.

Table S3. Comparison with other catalysts: photocatalytic procedure (risk type and E factor).[a]

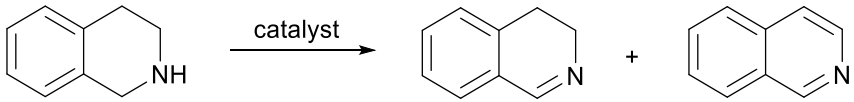

1 2 3

Entry (ref.)	Catalyst	Bio-accumulation[b]	Ecotoxicity[c]	Energy usage[d]/ Global warming[e]	Eutrophication[f]	Flammability	Human carcinogenicity	Persistence[g]	Water consumption	E factor[h]
1 (3)	Porphyrinic Zr-MOF			0.35	contains N			high Mw		180
2 (4)	Tetraphenylporphyrin			2.40	contains N					19
3 (7)	Chromophore-cobaloxime			0.58	contains N		THF	high Mw		126
4 (8)	Porous organic polymer			0.30	contains N			polymer high Mw		61
5 (10)	C_{70}			0.8 / $CHCl_3$			$CHCl_3$			156
6 (11)	CO_2, eosin Y	eosin Y log K_{ow} 4.80		0.58	contains N				in work-up	175
7 (13)	mpg-C_3N_4			0.60	contains N	MeCN, 80 °C[i]		polymer high Mw		67
8 (15)	$Bi_2O_2CO_3$			1.8					in work-up	91
9 (19)	Nb_2O_5		benzene	5.5			benzene			15
10 (20)	$MoS_2/ZnIn_2S_4$			0.54					co-solvent	143
11	TiO_2-P25			0.048						29[j]
12	CuNPs/TiO_2-P25			0.048						5[k]

[a] The information in the table refers only to the photocatalytic procedure; the work-up has been excluded except in the "Water consumption" column; the green colour means that the method is very probably exempt from that type of risk, whereas the yellow colour means that the method probably is not exempt from that type of risk; the information on bio-accumulation, ecotoxicity and human carcinogenicity is based on the Safety Data Sheet (SDS) of the compounds. [b] High risk to bio-accumulate if a compound has a log K_{ow} >4.3. [c] Ecotoxicity is a more severe risk factor if water-soluble compounds are required in relatively large amounts. [d] Energy usage in kWh, calculated from the number and power of the lamps/LEDs and the time of irradiation; procedures consuming >1 kWh have been highlighted in yellow; the rest in green colour have energy consumption <1kWh. [e] Includes the use of halogenated C1-C4 organics. [f] Medium risk for compounds containing N. [g] Compounds with high molecular weight, highly halogenated or polycyclic aromatic compounds (PACs). [h] The E factor has been estimated taking into account the amount of catalyst, solvent, additives and the amount of product; the work-up has been excluded because the amount of water or solvents used is not specified in all the procedures. Therefore, these values give only an approximate idea about the potential waste generated in the reaction. [i] MeCN has a flash point (6 °C) much lower than the operating temperature (80 °C). [j] Determined for one run because of the substantial drop in selectivity observed from the second run onward. [k] Determined for five runs with partial recovery of the solvent.

Table S4. Comparison with other catalysts: preparation of the catalyst (risk type, number of steps and recyclability).[a]

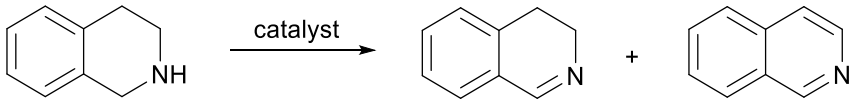

1 2 3

Entry (ref.)	Catalyst	Ecotoxicity[b]	Energy usage[c]	Eutrophication[d]	Flammability	Human carcinogenicity	Water consumption	Synthetic steps[e]	Catalyst reuse[f]
1 (3)	Porphyrinic Zr-MOF	DMF	85, 120, 140 ºC (40 h)	contains N	pyrrole,[g] 140 ºC	THF	co-solvent and in work-up	3 (12)	5[h]
2 (4)	Tetraphenylporphyrin (commercial)[i]	n/a	n/a	n/a	n/a	n/a	n/a	n/a	no
3 (7)	Chromophore-cobaloxime	DMF	40, 70 ºC (28 h) DMF distillation	contains N		CH_2Cl_2, THF	in work-up	4 (7)	no
4 (8)	Porous organic polymer		80 ºC (58 h)	contains N		CH_2Cl_2, $ClCH_2CH_2Cl$		2 (4)[j]	5[k]
5 (10)	C_{70} (commercial)[l]	n/a	n/a	n/a	n/a	n/a	n/a	n/a	3
6 (11)	CO_2, eosin Y (commercial)[m]	n/a	n/a	n/a	n/a	n/a	n/a	n/a	no
7 (13)	mpg-C_3N_4	NH_2CN	60, 70, 550 ºC (28 h)	contains N		NH_2CN	solvent and in work-up	1 (4)	4[h]
8 (15)	$Bi_2O_2CO_3$	CTAB		contains N			solvent and in work-up	1 (3)	5
9 (19)	Nb_2O_5 (commercial)[n]	n/a	n/a	n/a	n/a	n/a	n/a	n/a	2[o]
10 (20)	$MoS_2/ZnIn_2S_4$	$(NH_4)_2S$, $ZnCl_2$, $InCl_3$, thioacetamide	60, 200 ºC (48 h)	contains N		thioacetamide	solvent and in work-up	3 (9)	3
11	TiO_2-P25	n/a	n/a	n/a	n/a	n/a	n/a	n/a	–[p]
12	CuNPs/TiO_2-P25	$CuCl_2$				THF		1 (2)	5

[a] The information in the table refers only to the synthesis of the catalysts; the green colour means that the method is very probably exempt from that type of risk, whereas the yellow colour means that the method probably is not exempt from that type of risk; the information on bio-accumulation, ecotoxicity and human carcinogenicity is based on the Safety Data Sheet (SDS) of the compounds. [b] Ecotoxicity is a more severe risk factor if water-soluble compounds are required in relatively large amounts; compounds in a green background are used in relatively low amounts. [c] Procedures requiring prolonged heating or light sources ≥200 W have been considered; in parenthesis the total number of hours. [d] Medium risk for compounds containing N. [e] Synthetic steps are considered those leading to a different compound; the number of operations such as filtration, washing, drying, extraction, etc., is shown in parenthesis. [f] Number of cycles. [g] Pyrrole has a flash point (36 ºC) much lower than the operating temperature (140 ºC). [h] Reused in the oxidation of benzylamine to the corresponding imine. [i] 1g, 344 € (Sigma-Aldrich). [j] The starting monomer is not commercial; the number of operations needed to prepare it are not included. [k] Reused in the oxidation of thioanisole to the corresponding sulfoxide. [l] 500 mg, 591 € (Sigma-Aldrich). [m] 25 g, 682 € (Sigma-Aldrich). [n] 100 g, 198 € (Sigma-Aldrich). [o] Reused in the oxidation of 4-methoxybenzylamine to the corresponding imine. [p] The recycled catalyst showed an important drop in the selectivity already in the second run, which was much more pronounced in the third run.

14. References

1. (a) S. Valencia, J. M. Marin and G. Restrepo. Study of the bandgap of synthesized titanium dioxide nanoparticules using the sol-gel method and a hydrothermal treatment. *Open Mater. Sci. J.*, 2010, **4**, 9–14. (b) R. López and R. Gómez. Band-gap energy estimation from diffuse reflectance measurements on sol–gel and commercial TiO_2: a comparative study. *J. Sol–Gel Sci. Technol.*, 2012, **61**, 1–7.
2. A. B. Murphy. Band-gap determination from diffuse reflectance measurements of semiconductor films, and application to photoelectrochemical water-splitting. *Sol. Energy Mater. Sol. Cells*, 2007, **91**, 1326–1337, and the references therein.
3. C. Xu, H. Liu, D. Li, J.-H. Su and H.-L. Jiang. Direct evidence of charge separation in a metal–organic framework: efficient and selective photocatalytic oxidative coupling of amines via charge and energy transfer. *Chem. Sci.*, 2018, **9**, 3152–3158.
4. G. Jiang, J. Chen, J.-S. Huang and C.-M. Che. Highly efficient oxidation of amines to imines by singlet oxygen and its application in Ugi-type reactions. *Org. Lett.*, 2009, **11**, 4568–4571.
5. J. Jin, C. Yang, B. Zhang and K. Deng. Selective oxidation of amines using O_2 catalysed by cobalt thioporphyrazine under visible light. *J. Catal.*, 2018, **361**, 33–39.
6. K. Marui, A. Nomoto, H. Akashi and A. Ogawa. Green oxidation of amines to imines based on the development of novel catalytic systems using molecular oxygen or hydrogen peroxide. *Synthesis*, 2016, **48**, 31–42.
7. D. Chao and M. Zhao. A supramolecular assembly bearing an organic TADF chromophore: synthesis, characterisation and light-driven cooperative acceptorless dehydrogenation of secondary amines. *Dalton Trans.*, 2019, **48**, 5444–5449.
8. Y. Zhi, K. Li, H. Xia, M. Xue, Y. Mu and X. Liu. Robust porous organic polymers as efficient heterogeneous organo-photocatalysts for aerobic oxidation reactions. *J. Mater. Chem. A*, 2017, **5**, 8697–8704.
9. C. Su, R. Tandiana, B. Tian, A. Sengupta, W. Tang, J. Su and K. P. Loh. Visible-light photocatalysis of aerobic oxidation reactions using carbazolic conjugated microporous polymers. *ACS Catal.*, 2016, **6**, 3594–3599.
10. R. Kumar, E. H. Gleißner, E. G. V. Tiu and Y. Yamakoshi. C_{70} as a photocatalyst for oxidation of secondary benzylamines to imines. *Org. Lett.*, 2016, **18**, 184–187.
11. D. Riemer, W. Schilling, A. Goetz, Y. Zhang, S. Gehrke, I. Tkach, O. Hollóczki and S. Das. CO_2-catalysed efficient dehydrogenation of amines with detailed mechanistic and kinetic studies. *ACS Catal*, 2018, **8**, 11679–11687.

12. L. Huang, J. Zhao, S. Guo, C. Zhang and J. Ma. Bodipy derivatives as organic triplet photosensitizers for aerobic photoorganocatalytic oxidative coupling of amines and photooxidation of dihydroxylnaphthalenes. *J. Org. Chem.*, 2013, **78**, 5627–5637.
13. F. Su, S. C. Mathew, L. Möhlmann, M. Antonietti, X. Wang and S. Blechert. Aerobic oxidative coupling of amines by carbon nitride photocatalysis with visible light. *Angew. Chem. Int. Ed.*, 2011, **50**, 657–660.
14. S. Juntrapirom, S. Anuchai, O. Thongsook, S. Pornsuwan, P. Meepowpan, P. Thavornyutikarn, S. Phanichphant, D. Tantraviwat and B. Inceesungvorn. Photocatalytic activity enhancement of g-C_3N_4/BiOBr in selective transformation of primary amines to imines and its reaction mechanism. *Chem. Eng. J.*, 2020, **394**, 124934.
15. P. Bai, X. Tong, J. Wan, Y. Gao and S. Xue. Flower-like $Bi_2O_2CO_3$-mediated selective oxidative coupling processes of amines under visible light irradiation. *J. Catal.*, 2019, **374**, 257–265.
16. H. Li, Y. Yang, C. He, L. Zeng and C. Duan. Mixed-ligand metal–organic framework for two-photon responsive photocatalytic C–N and C–C coupling reactions. *ACS Catal.*, 2019, **9**, 422–430.
17. D. K. Tiwari, R. A. Maurya and J. B. Nanubolu. Visible-light/photoredox-mediated sp^3 C-H functionalization and coupling of secondary amines with vinyl azides in flow microreactors. *Chem. Eur. J.*, 2016, **22**, 526–530.
18. F. Stanek, R. Pawlowski, P. Morawska, R. Bujok and M. Stodulski. Dehydrogenation and α-functionalization of secondary amines by visible-light-mediated catalysis. *Org. Biomol. Chem.*, 2020, **18**, 2103–2112.
19. S. Furukawa, Y. Ohno, T. Shishido, K. Teramura and T. Tanaka. Selective amine oxidation using Nb_2O_5 photocatalyst and O_2. *ACS Catal.*, 2011, **1**, 1150–1153.
20. M. Hao, X. Deng, L. Xu and Z. Li. Noble metal free MoS_2/$ZnIn_2S_4$ nanocomposite for acceptorless photocatalytic semi-dehydrogenation of 1,2,3,4-tetrahydroisoquinoline to produce 3,4-dihydroisoquinoline. *Appl. Catal. B: Environ.*, 2019, **252**, 18–23.
21. X. Lang, W. Ma, Y. Zhao, C. Chen, H. Ji and J. Zhao. Visible-light-induced selective photocatalytic aerobic oxidation of amines into imines on TiO_2. *Chem. Eur. J.*, 2012, **18**, 2624–2631.
22. P. Bai, X. Tong, Y. Gaoa and P. Guoa. Oxygen-free water-promoted selective photocatalytic oxidative coupling of amines. *Catal. Sci. Technol.*, 2019, **9**, 5803–5811.
23. N. O. Balayeva, N. Zheng, R. Dillert and D. W. Bahnemann. Visible-light-mediated photocatalytic aerobic dehydrogenation of n-heterocycles by surface-grafted TiO_2 and 4-amino-TEMPO. *ACS Catal.* 2019, **9**, 10694–10704
24. N. O. Balayeva, Z. Mamiyev, R. Dillert, N. Zheng and D. W. Bahnemann. Rh/TiO_2-photocatalysed acceptorless dehydrogenation of N-heterocycles upon visible-light illumination. *ACS Catal.* 2020, **10**, 5542–5553.

15. NMR spectra

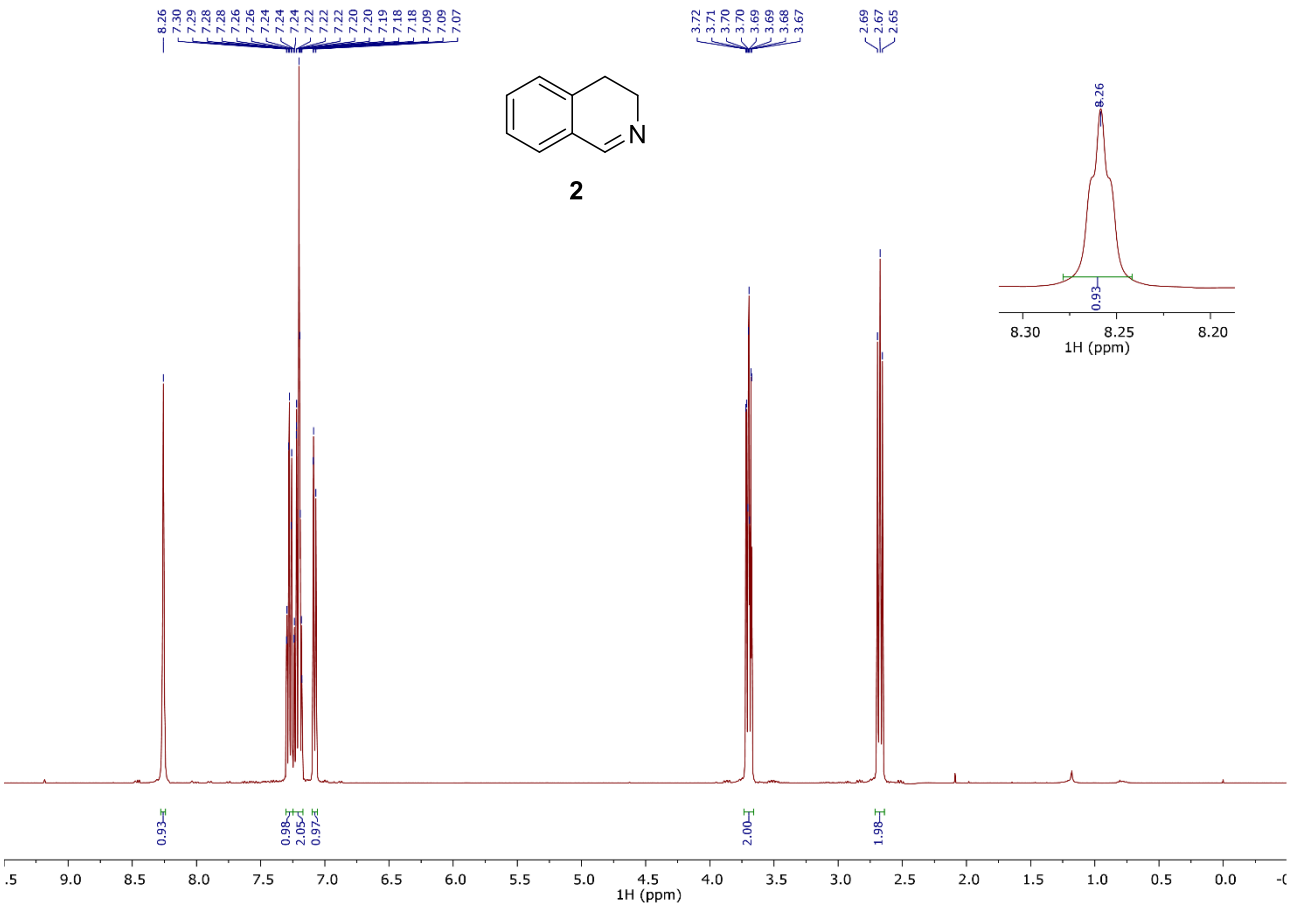

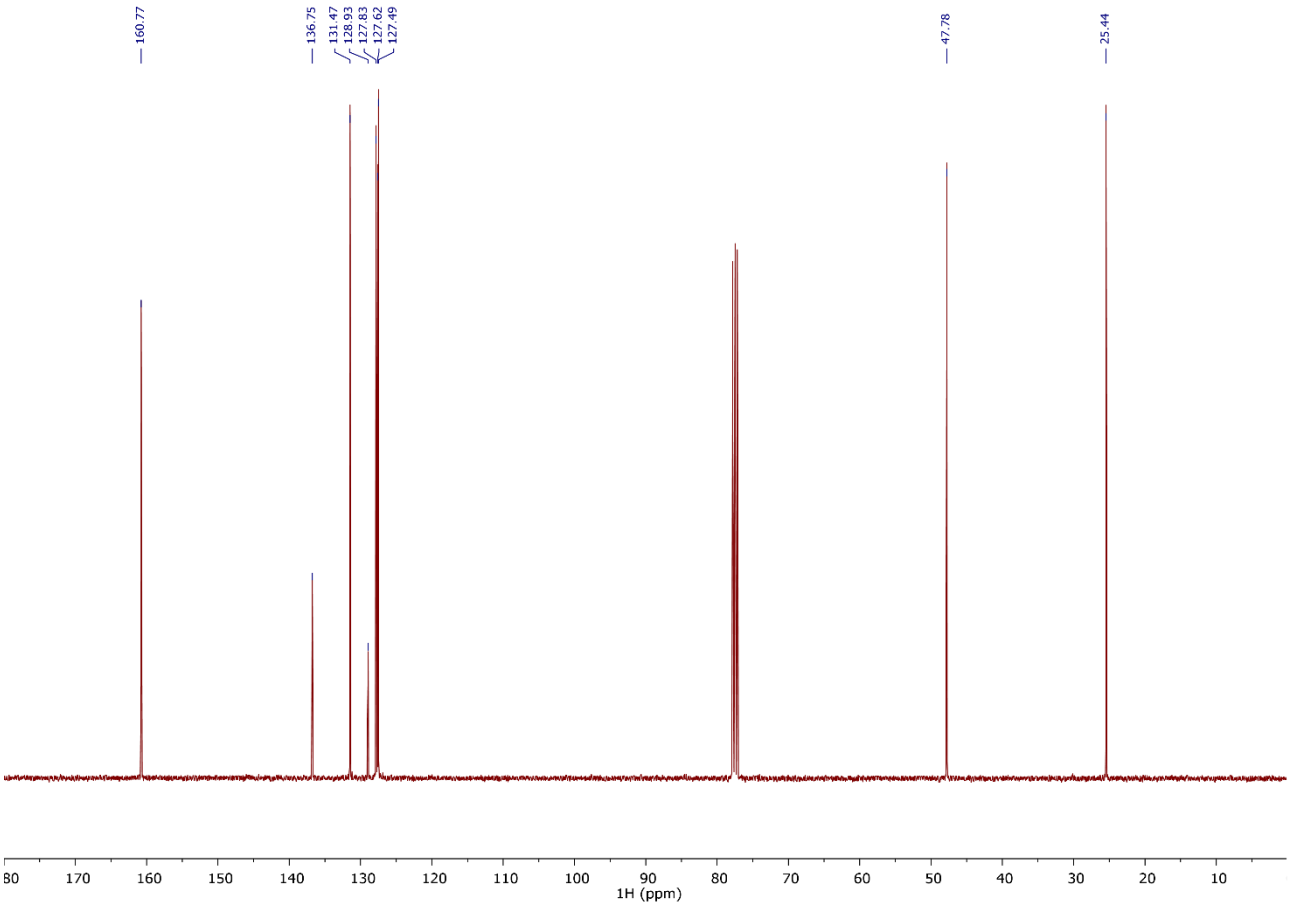

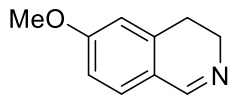
MeO
N

4

7.22
7.20
6.70
6.68
6.68
6.62
3.76
3.11
2.76
2.73
2.72
1.00
2.06
1.04
2.75
1.75
2.43
f1 (ppm)

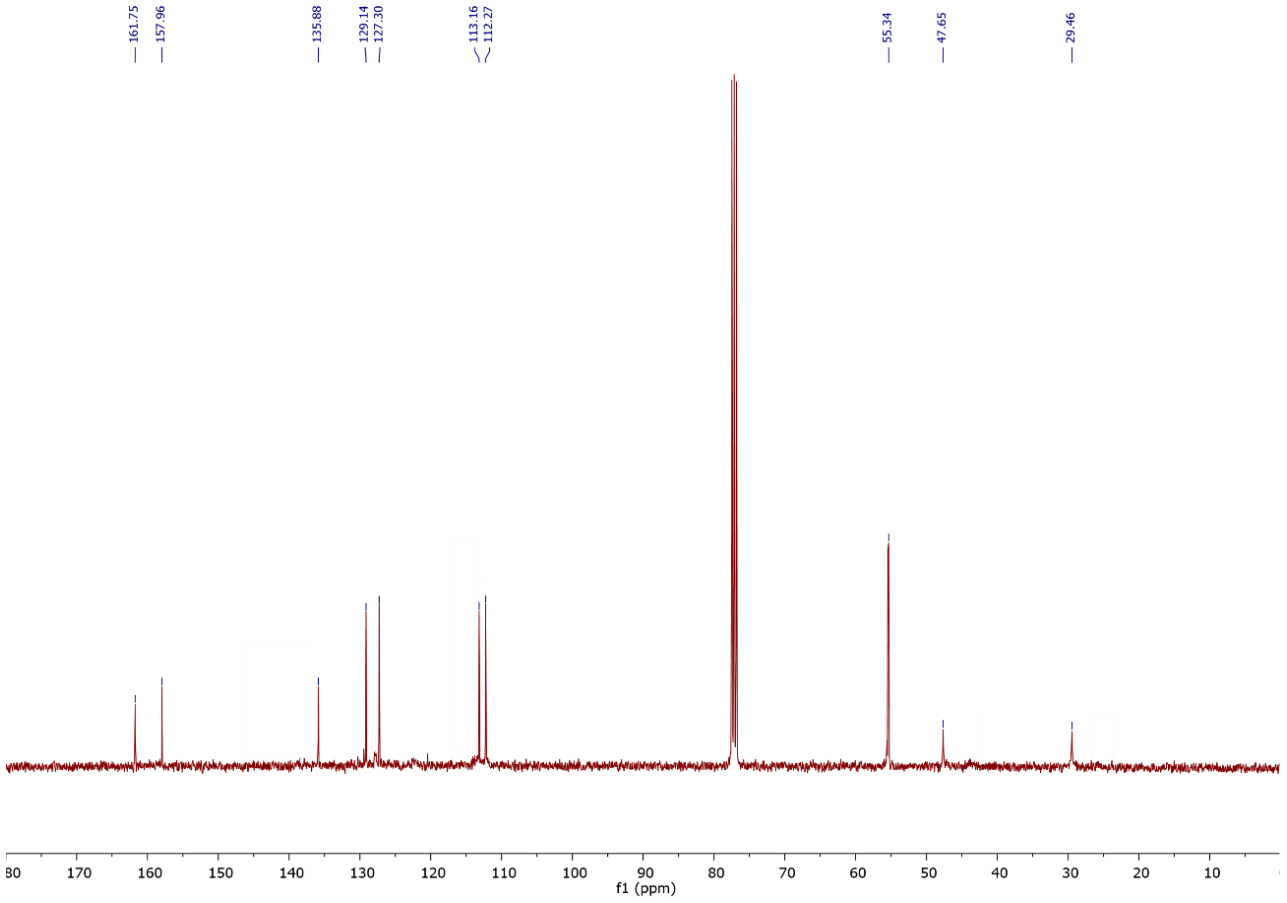
161.75
157.96
135.88
129.14
127.30
113.16
112.27
55.34
47.65
29.46
f1 (ppm)

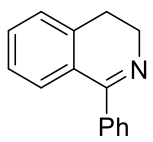
N
Ph

5

7.25
7.24
7.22
7.20
7.19
7.17
7.16
7.14
3.79
3.77
3.75
2.77
2.74
2.72
2.70
9.33
1.65
2.00
f1 (ppm)

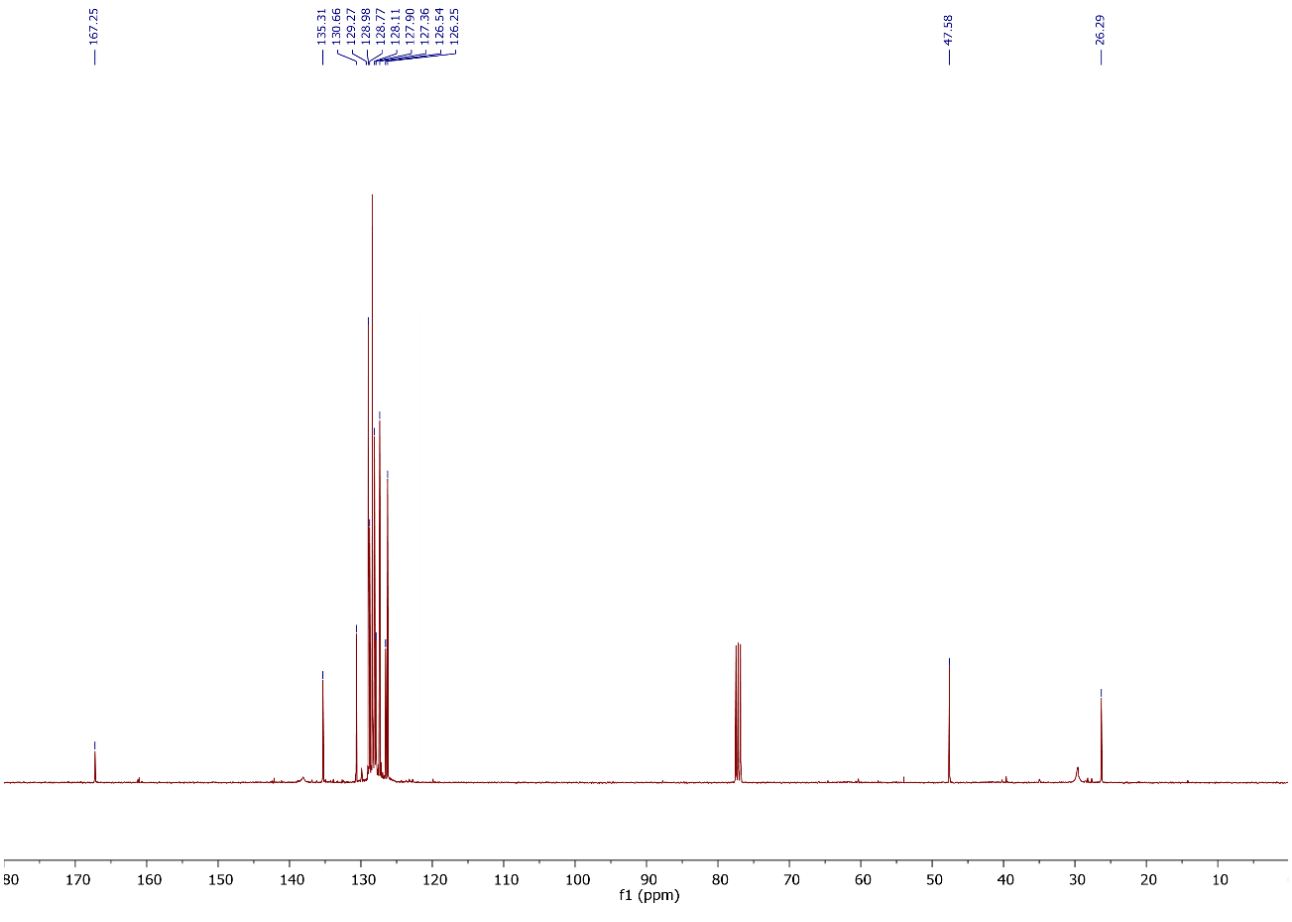
167.25
135.31
130.66
129.27
128.98
128.77
128.11
127.90
127.36
126.54
126.25
47.58
26.29
f1 (ppm)

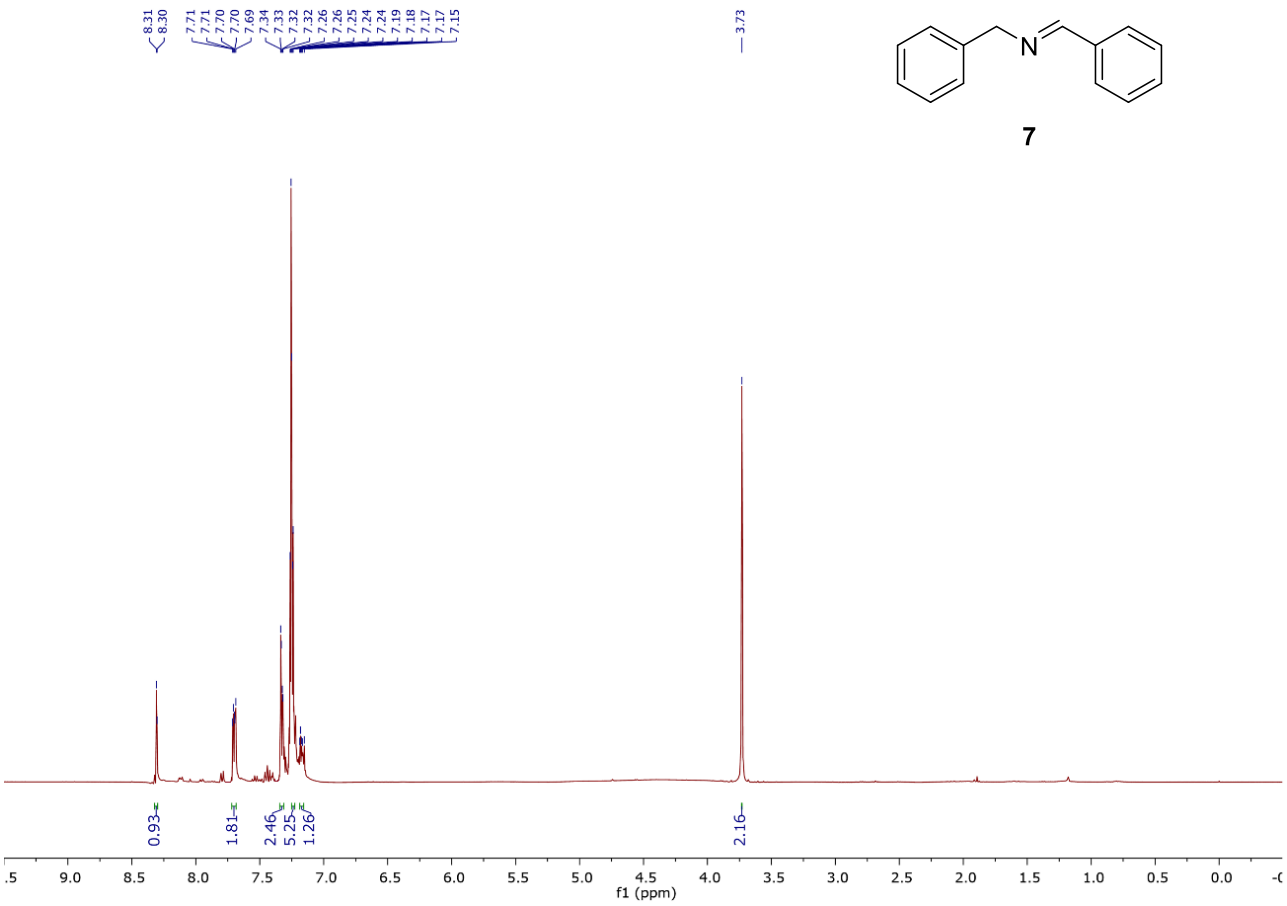
8.31
8.30
7.71
7.71
7.70
7.70
7.69
7.34
7.33
7.32
7.32
7.26
7.26
7.25
7.24
7.24
7.19
7.18
7.17
7.17
7.15
3.73
0.93
1.81
2.46
5.25
1.26
2.16
f1 (ppm)

7

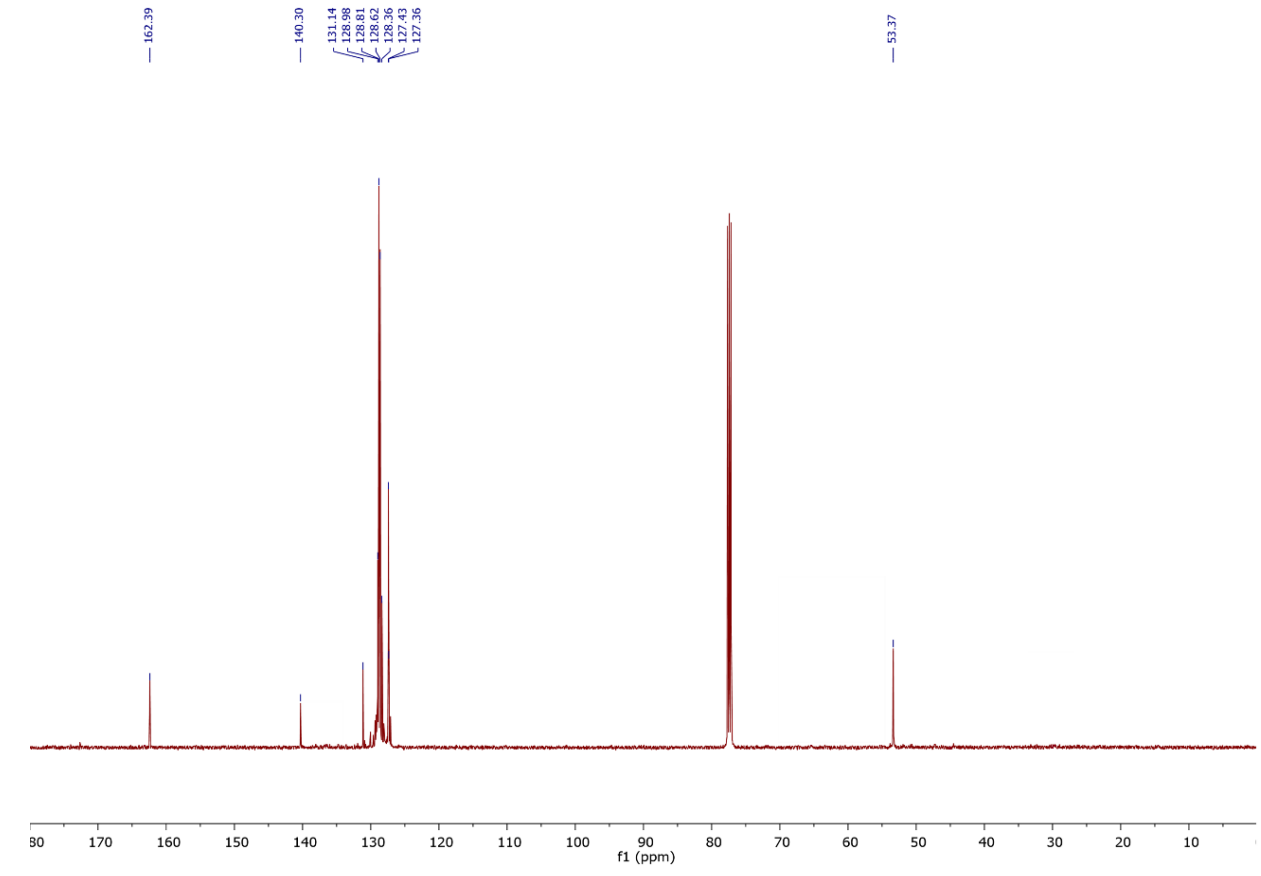
162.39
140.30
131.14
128.98
128.81
128.62
128.36
127.43
127.36
53.37
f1 (ppm)

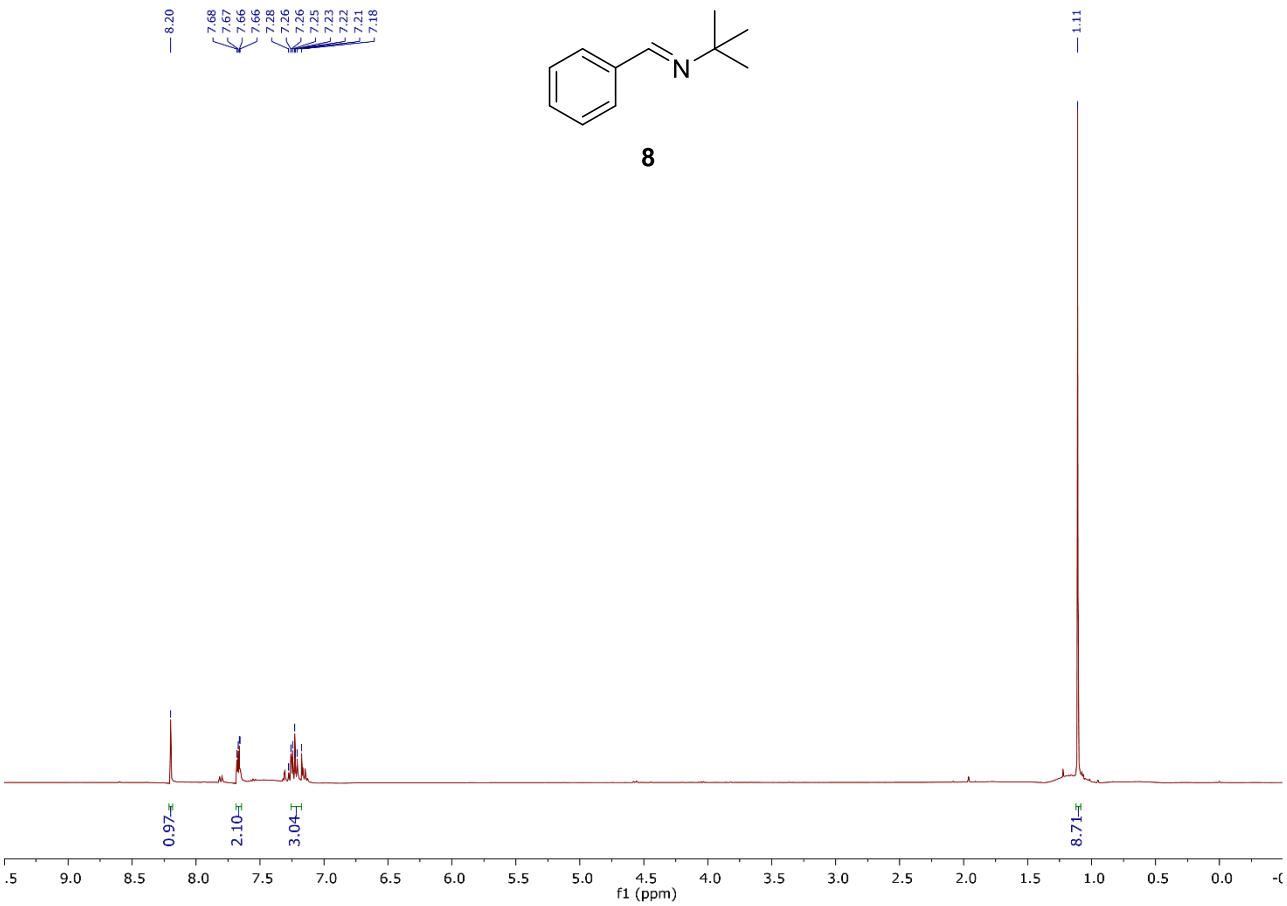
8.20
7.68
7.67
7.66
7.66
7.28
7.26
7.26
7.25
7.23
7.22
7.21
7.18
1.11
N
0.97
2.10
3.04
8.71
f1 (ppm)

8

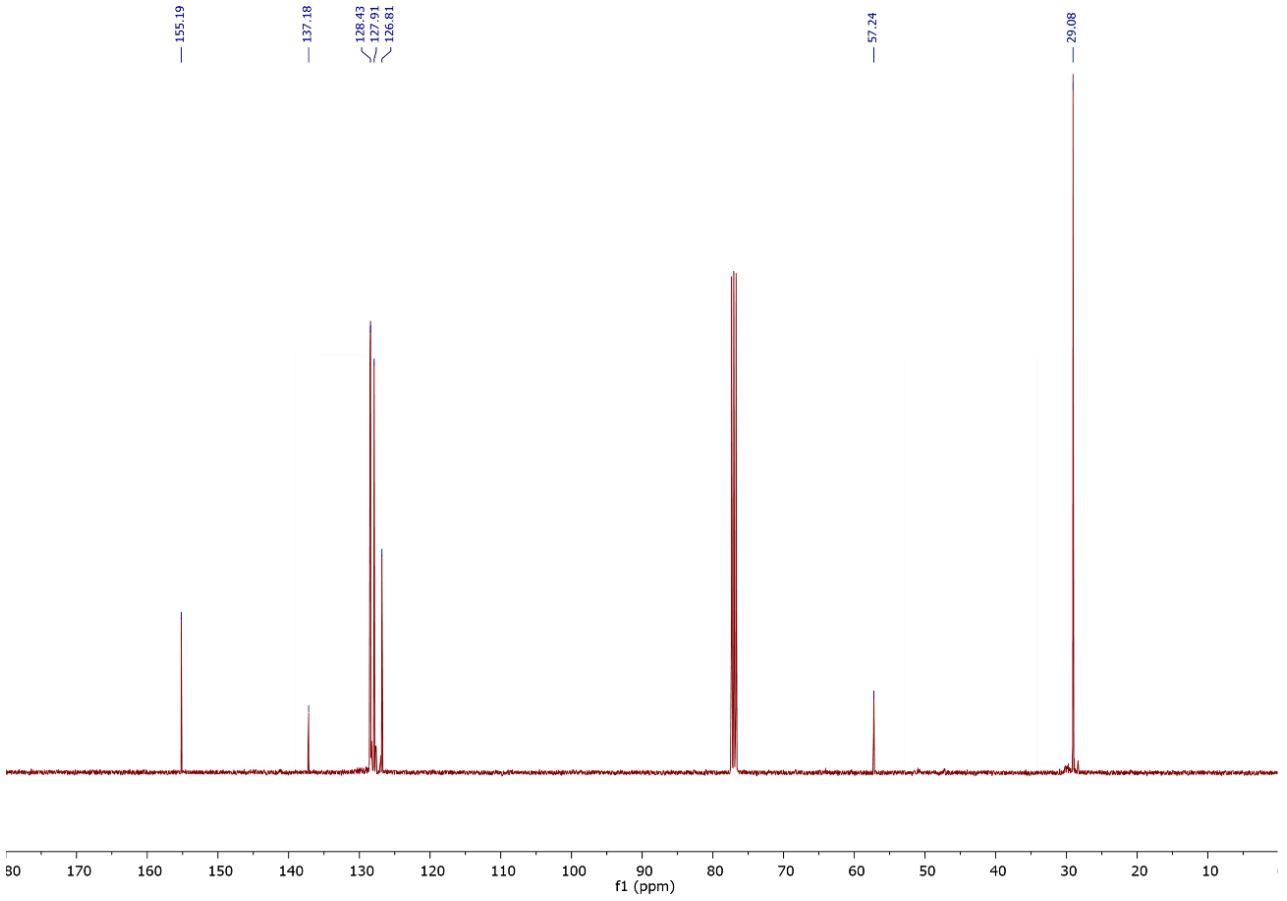
155.19
137.18
128.43
127.91
126.81
57.24
29.08
f1 (ppm)

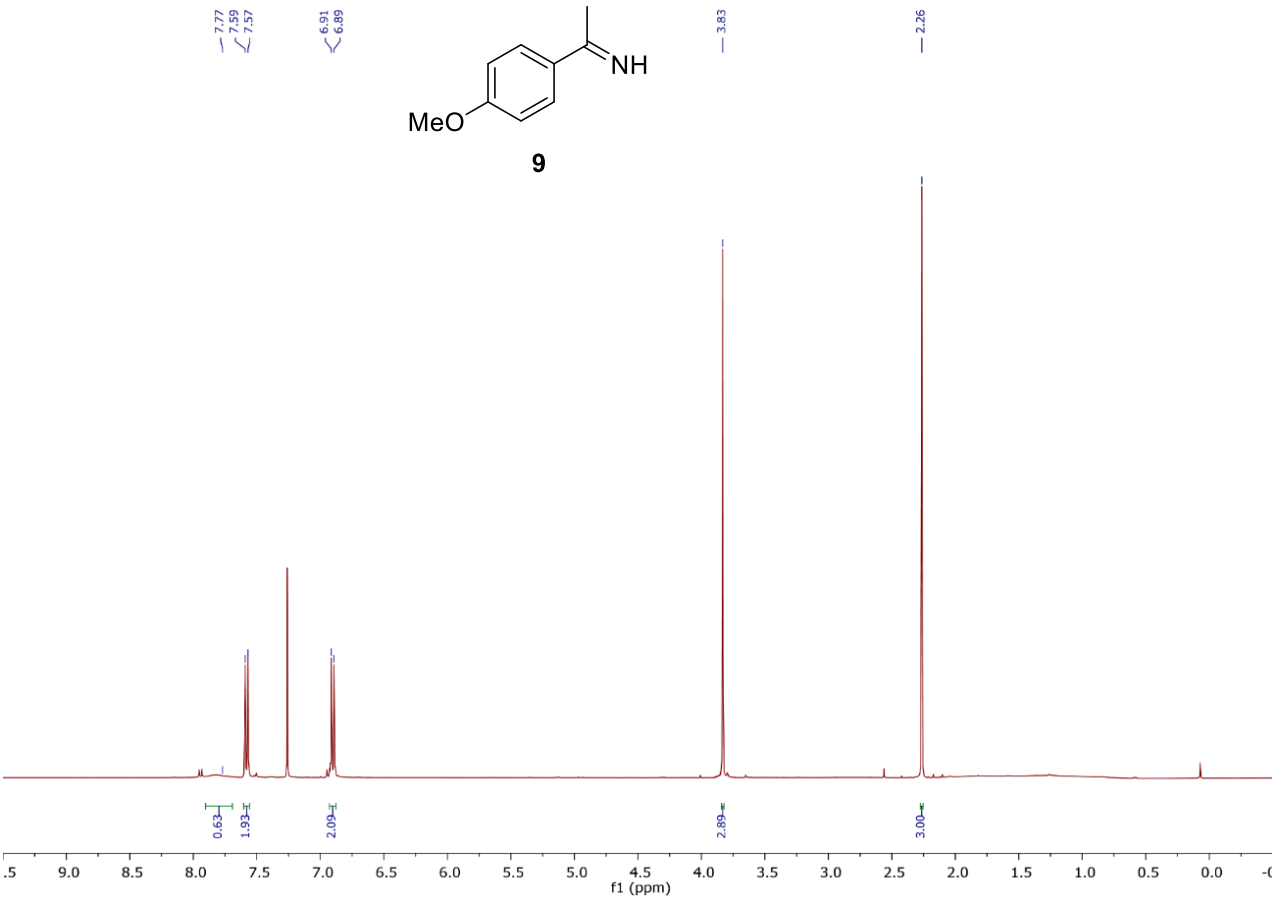
7.77
7.59
7.57
6.91
6.89
3.83
2.26
NH
MeO
0.63
1.93
2.09
2.89
3.00
f1 (ppm)

9

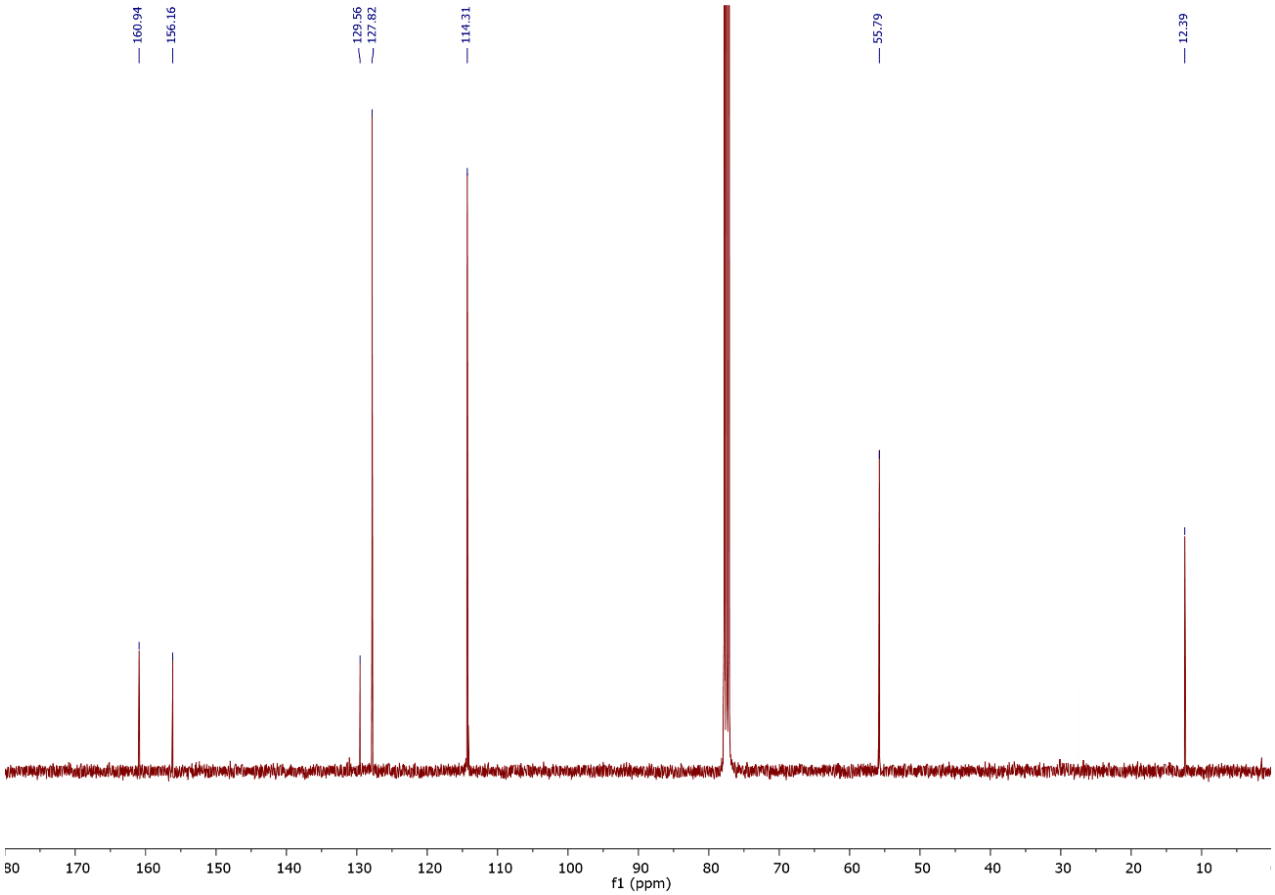
160.94
156.16
129.56
127.82
114.31
55.79
12.39
f1 (ppm)

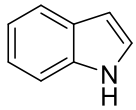

10


7.88
7.58
7.57
7.56
7.55
7.26
7.25
7.24
7.23
7.13
7.12
7.11
7.11
7.10
7.09
7.09
7.06
7.05
7.04
7.03
7.03
7.02
7.02
7.02
6.46
6.46
6.46
6.45
6.45
6.45

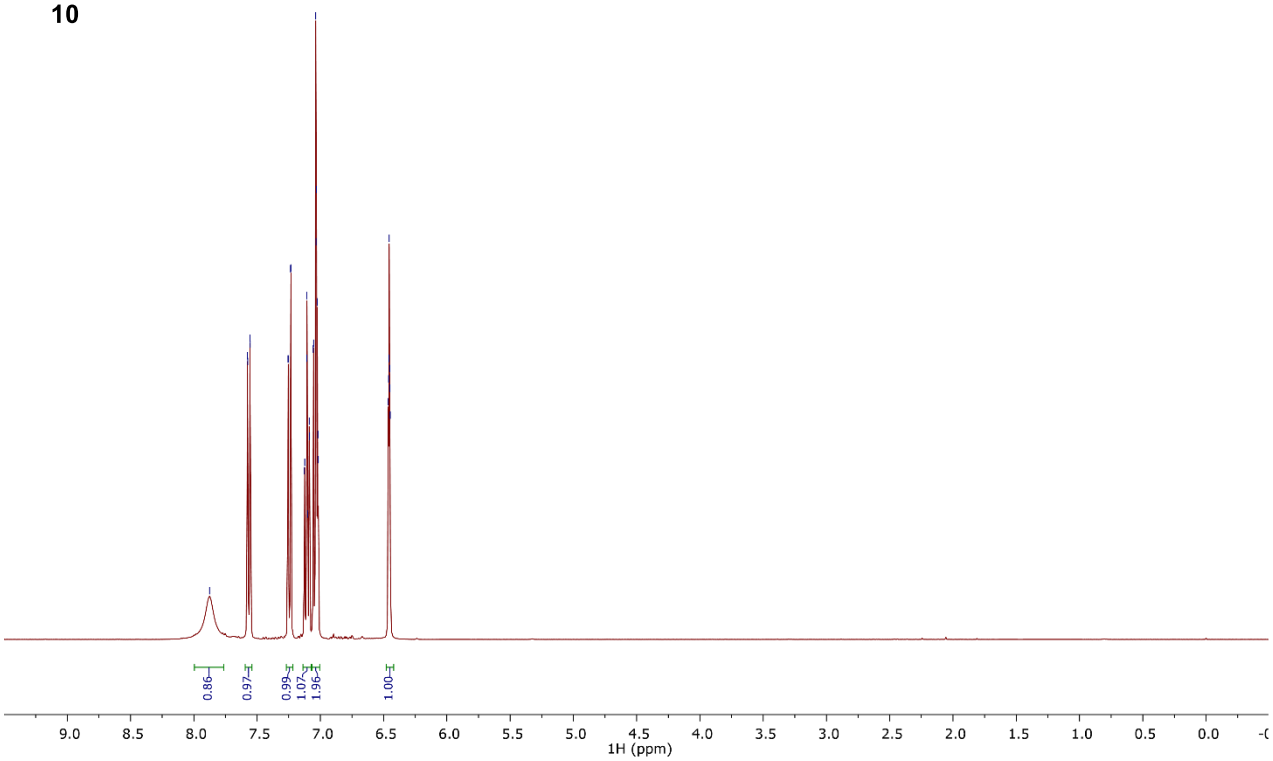
0.86
0.97
0.99
1.07
1.96
1.00
9.0
8.5
8.0
7.5
7.0
6.5
6.0
5.5
5.0
4.5
4.0
3.5
3.0
2.5
2.0
1.5
1.0
0.5
0.0
1H (ppm)

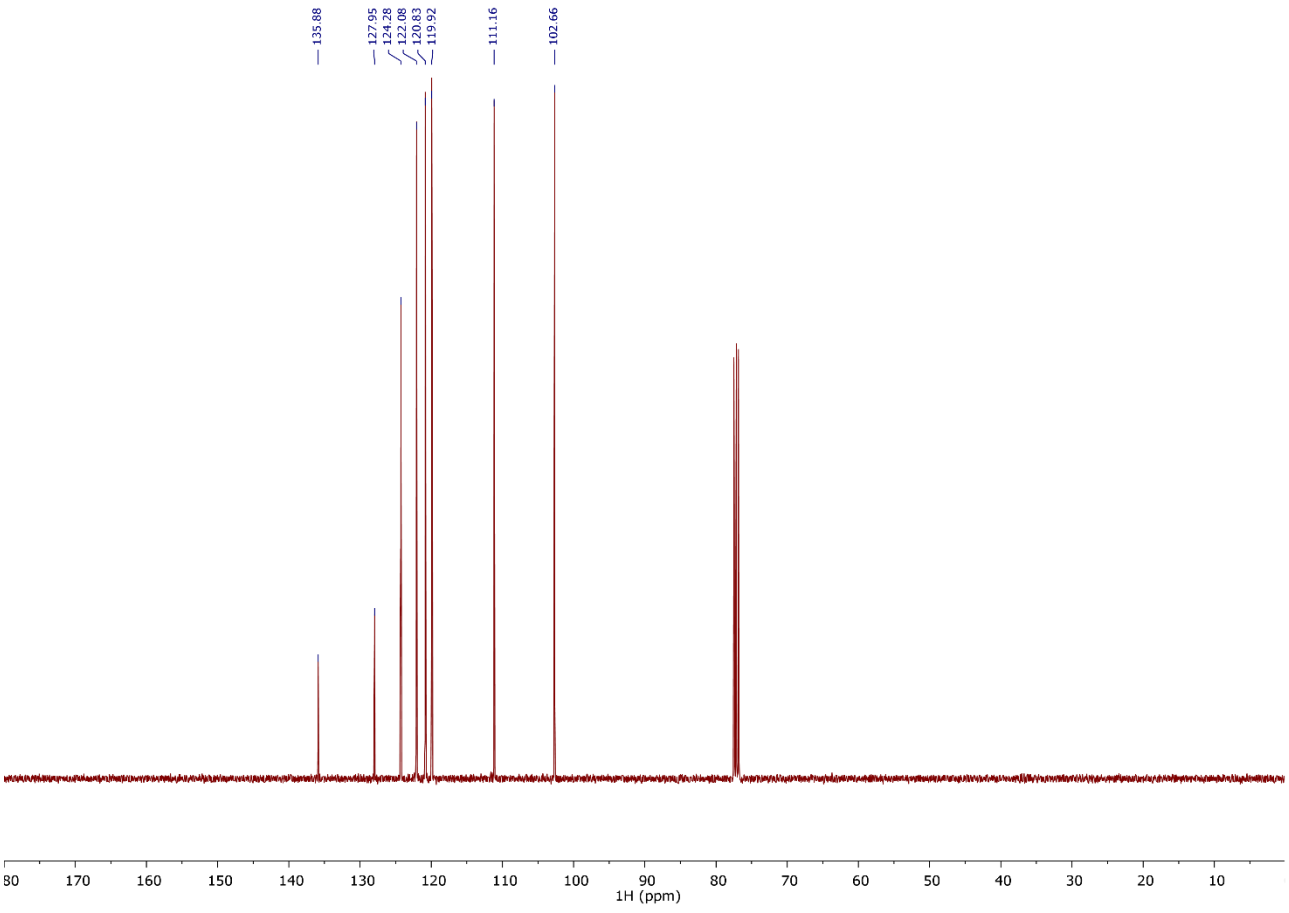
135.88
127.95
124.28
122.08
120.83
119.92
111.16
102.66
180
170
160
150
140
130
120
110
100
90
80
70
60
50
40
30
20
10
1H (ppm)